Fuel 360 (2024) 130618

Contents lists available at ScienceDirect

Fuel

journal homepage: www.elsevier.com/locate/fuel

Full length article

Impact of medium-pressure direct injection in a spark-ignition engine fueled by hydrogen

S. Molina, R. Novella, J. Gomez-Soriano *, M. Olcina-Girona

CMT – Clean Mobility & Thermofluids, Universitat Politècnica de València, Camino de Vera s/n, 46022 Valencia, Spain

ARTICLE INFO

Keywords:
Hydrogen fuel
Direct injection
Port fuel injection
Lean combustion
Spark-ignition engine

ABSTRACT

In the automotive sector, hydrogen is being increasingly explored as an alternative fuel to replace conventional carbon-based fuels. Its combustion characteristics make it well-suited for adaptation to internal combustion engines. The wide flammability range of hydrogen allows for higher dilution conditions, resulting in enhanced combustion efficiency. When combined with lean combustion strategies, hydrogen significantly reduces environmental impact, virtually eliminating carbon dioxide and nitrogen oxide emissions while maintaining high thermal efficiency. This paper aims to assess the potential of using an outwardly opening poppet valve hydrogen direct injection (DI) system in a small engine for light-duty applications. To achieve this, a comparison of performance, emission levels, and combustion parameters is conducted on a single-cylinder spark-ignition (SI) research engine fueled by hydrogen, using both port fuel injection (PFI) and this new direct injection system. Two different engine loads are measured at multiple air dilution and injection timing conditions. The results demonstrate notable efficiency improvements, ranging from 0.6% to 1.1% when transitioning from PFI to DI. Accurate control of injection timing is essential for achieving optimal performance and low emissions. Delaying the start of injection results in a 7.6% reduction in compression work at low load and a 3.9% reduction at high load. This results in a 3.1-3.2% improvement in ISFC in both load conditions considered.

1. Introduction

Reducing greenhouse gas (GHG) emissions is crucial to mitigating the global warming effect. The European Union (EU) aims to achieve zero net greenhouse gas emissions by 2050 through the planned Green Deal program. By 2030, the interim target is to reduce GHG emissions by 55% compared to 1990 levels. However, as of 2020, only a 20% decrease had been accomplished, highlighting the need for significantly greater efforts to achieve the goal.

Transportation represents a substantial source of GHG emissions, accounting for approximately 32% of the carbon dioxide (CO_2) emissions in Europe [1]. Furthermore, the escalation persists despite the implementation of new environmental regulations and the advancement of more efficient vehicle technologies. Hence, a potential solution to the problem lies in diversifying future fuels [2,3], emphasizing the development of CO_2 neutral powertrains that also minimize emissions of other pollutant exhaust components [4,5].

Hydrogen (H_2) fuel possesses properties that align with the needs of the automotive transportation sector. It exhibits approximately six times the combustion speed of gasoline, a wide flammability range, and serves as a carbon-free fuel. These characteristics indicate that hydrogen is a suitable fuel for achieving optimal engine performance while minimizing GHG and pollutant emissions. Moreover, hydrogen production can be coupled with renewable energy sources (RES) [6,7], facilitating its integration into the grid as an energy vector. Power-to-gas (P2G) systems, which convert surplus renewable energy into hydrogen gas through electrolysis, become a viable option only when they serve as the sole means of achieving a high share of RES. The current natural gas grid has the potential to accommodate hydrogen as an energy vector in the transition towards a fully renewable energy system [8].

The use of H_2 as fuel for transportation through internal combustion engines (ICEs) has been the subject of research for decades. It has been employed as an additive to enhance the combustion characteristics of other fuels, such as gasoline [9,10] or compressed natural gas (CNG) [11]. This approach has proven effective in reducing pollutant emissions, increasing fuel efficiency, and improving engine performance. Furthermore, studies have explored the possibility of onboard hydrogen generation within a vehicle through the reforming of a portion of the primary fuel [12]. This method enables on-demand hydrogen production, eliminating the need for dedicated hydrogen storage tanks with a limited range [13].

* Corresponding author.
E-mail address: jogoso1@mot.upv.es (J. Gomez-Soriano).

https://doi.org/10.1016/j.fuel.2023.130618
Received 8 September 2023; Received in revised form 17 November 2023; Accepted 11 December 2023
Available online 14 December 2023

Glossary

BTE	Brake Thermal Efficiency
CA10	Combustion after 10% of fuel burnt
CA50	Combustion after 50% of fuel burnt
CA90	Combustion after 90% of fuel burnt
CAD	Crank Angle Degrees
CCV	Cycle-to-Cycle Variation
CLD	Cadmium Luminescence Detector
CNG	Compressed Natural Gas
CO	Carbon Monoxide
CO_2	Carbon Dioxide
COV_{IMEP}	IMEP coefficient of variation
EGR	Exhaust Gas Recirculation
EVC	Exhaust Valve Closing
EVO	Exhaust Valve Opening
EU	European Union
FID	Flame Ionization Detector
GIE	Gross Indicated Efficiency
GHG	Greenhouse Gases
H_2	Hydrogen
H2-DI	Hydrogen Direct Injection
HC	Hydrocarbons
HICE	Hydrogen Internal combustion Engine
HRR	Heat Release Rate
ICE	Internal Combustion Engine
IMEP	Indicated Mean Effective Pressure
ISCO	Indicated specific CO
$ISCO_2$	Indicated specific CO_2
ISFC	Indicated specific fuel consumption
ISHC	Indicated specific HC
$ISNO_x$	Indicated specific NO_x
ITE	Indicated Thermal Efficiency
IVO	Intake Valve Opening
IVC	Intake Valve Closing
NDIR	Non-Dispersive Infrared Spectroscopy
NO_x	Nitrogen Oxides
O_2	Oxygen
P2G	Power-to-gas
PFI	Port Fuel Injection
PLIF	Planar Laser-Induced Fluorescence
PMA	Magneto-Pneumatic Analysis
RES	Renewable Energy Sources
RON	Research Octane Number
SD	Standard Deviation
SI	Spark-ignition
ST	Spark Timing
SOC	Start of Combustion
SoI	Start of Injection
TDC	Top Dead Center

When H_2 is used as the sole fuel, operating under high dilution conditions proves beneficial in reducing knock susceptibility [14], nitrogen oxides (NO_x) emissions [15], and improving engine performance and efficiency [16–18]. However, several issues are associated with the utilization of hydrogen in internal combustion engines. These issues include the presence of high-pressure rise caused by combustion instabilities [19,20], the occurrence of pre-ignition or knocking within the combustion chamber [20,21], and the sequential progression of pre-ignition and backfire into the intake manifold [22,23], particularly under high load conditions. The prevention of these abnormal combustion events is a crucial factor in ensuring the long-term durability of powerplants [24]. Recent studies have evaluated the impact of dilution in a medium-duty engine for transport applications [25]. Shi et al. [26] have recently studied the effect of water injection in a rotary engine, demonstrating a reduction in knock propensity and NO_x mitigation as the amount of injected water increases.

The delivery of hydrogen to an engine can be performed through various injection systems, with the most commonly employed ones being port fuel injection (PFI) and direct injection (DI). PFI involves injecting fuel into the inlet manifold, whereas DI involves injecting fuel directly into the combustion chamber. Port fuel injection hydrogen systems have limitations regarding volumetric efficiency and a higher probability of abnormal combustion events [27]. Conversely, direct injection hydrogen systems can overcome volumetric drawbacks but may necessitate specialized and expensive engine components [28].

Recent studies have showcased the potential of hydrogen direct injection (H2-DI) in attaining remarkable performance and efficiency [29]. Through precise control of the intake valve closing and exhaust valve opening timing, researchers achieved an impressive brake thermal efficiency (BTE) of 42.2% [30]. Furthermore, the characterization of knock intensity in H2-DI was also investigated [31].

The direct injection process induces higher in-cylinder turbulence and stratification compared to the premixed charge PFI counterpart, leading to accelerated fuel combustion [28]. It was observed that the variation in knock intensity is non-linear with the retardation of the start of injection (SoI), which can be attributed to the distribution of the cylinder mixture. Several researchers [32,33] investigated mixture formation in an optically accessible hydrogen-fueled engine. By employing Planar Laser-Induced Fluorescence (PLIF), they discovered that injector tip geometry, injector location, injection timing, nozzle design, and injector geometry are critical parameters affecting the in-cylinder mixing process in direct-injection HICE. Eichlseder et al. [34] discovered that at low equivalence ratios, the indicated thermal efficiency (ITE) increases with a delay in the start of injection (SoI). This increase is attributed to a reduction in compression work resulting from variations in mixture gas properties and charge mass associated with a delayed SoI. However, Kim et al. [35] present conflicting results to those of Eichlseder et al. [34]. They found that for both low and high loads, thermal efficiency decreases consistently as the SoI is delayed. In a multi-cylinder automotive engine, Kim et al. [36] observed a 30% increase in power density when transitioning from PFI to DI while maintaining the same brake thermal efficiency with delayed ignition timings. Similarly, Maio et al. [37] observed equivalent trends in a single-cylinder heavy-duty engine.

These contradictory findings could potentially be attributed to variations in mixture formation. This perspective is supported by the findings of Shudo et al. [38], who demonstrated that by implementing charge stratification in a manner that promotes a lean local mixture fraction near the wall region compared to the overall mixture, significant reductions in cooling losses can be achieved alongside improved thermal efficiency. These findings have arisen in the context of SI engines using gasoline direct injection (GDI) systems loosely adapted for extensive use with hydrogen as fuel and complying with the necessary safety measures for vehicle use. In this type of injector, fuel is introduced into the combustion chamber through single or multiple cylindrical or conical nozzles, exhibiting the conventional injection patterns observed in gasoline-based engines.

However, from a technological development perspective, there is a new trend towards using gas-based injectors due to their advantages in terms of safety and control [39]. Unlike conventional DI injectors, whether single- or multi-hole with inwardly opening designs and cylindrical nozzles, which are susceptible to opening under cylinder pressure if the injection pressure is lower, gas-based injectors inject hydrogen through an outwardly opening poppet valve. This results in entirely

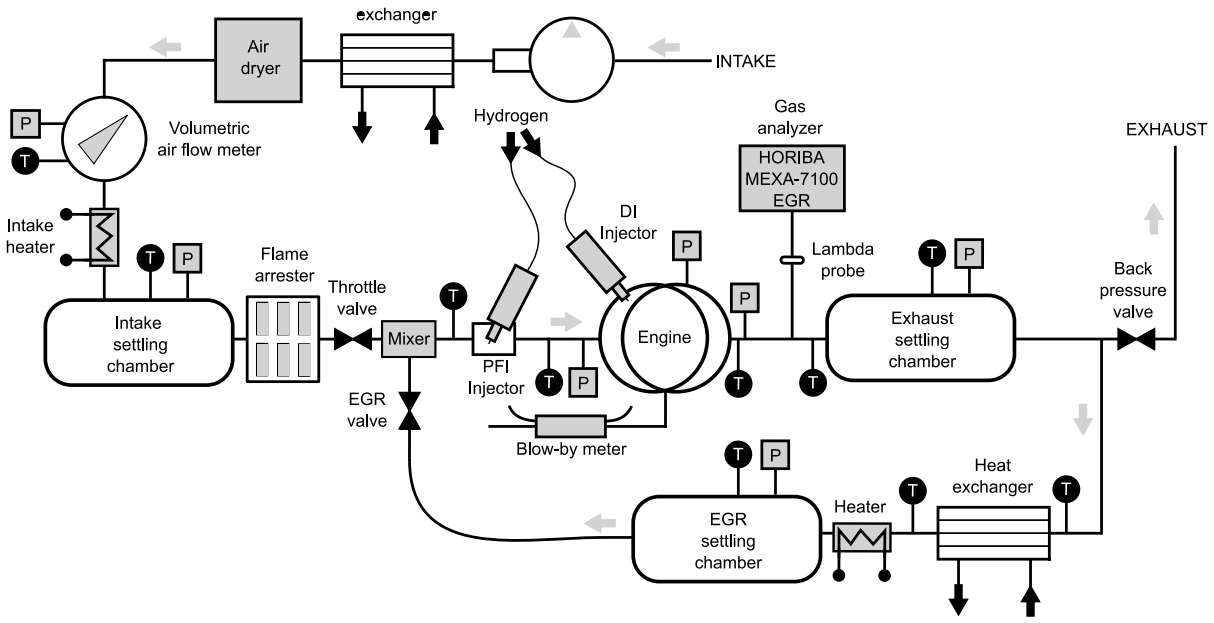

Fig. 1. Experimental engine layout.

different spray patterns and mixture rates [40]. These latter parameters are directly related to the injection channel design and are completely distinct from those observed in conventional GDI nozzles [41].

None of the works conducted to date have employed a combination of a modern engine platform and an outwardly opening poppet valve gas direct injector. While numerous studies exist that assess the impact of direct injection on modern, small-displacement, turbocharged engines with new combustion chamber designs, all of them use GDI-adapted injectors with single or multiple cylindrical nozzles to supply hydrogen into the combustion chamber. Therefore, further research is needed to explore how this kind of hydrogen injection system impacts combustion, emissions, and engine performance under different dilutions and operating conditions.

This study aims to contribute to the existing knowledge regarding the effects of mixture formation by utilizing different injection strategies. It seeks to assist in advancing current technology for implementing hydrogen as a fuel in light road transportation applications. The authors conducted an extensive experimental campaign using a single-cylinder spark-ignition research engine for light-duty applications to analyze the performance, combustion process, and emissions when the engine is equipped with two outwardly opening poppet valve hydrogen injectors (PFI and DI) under various levels of air dilution. Additionally, the impact of mixture stratification is evaluated by manipulating the injection timing of the DI system, transitioning from lean homogeneous charge to lean stratified charge combustion mode.

2. Material and methods

This section describes the experimental tools and methods used in the investigation to give a clear and concise understanding of the experiment procedures and the processing methodology.

2.1. Experimental tools

The experiments were conducted on a single-cylinder SI engine with a displacement of 454.2 cm^3. The experimental facilities were previously utilized in the investigation performed by Molina et al. [42,43]. The main engine specifications are listed in Table 1 for reference. The engine featured an 86-mm stroke with a compression ratio (CR) of 10.7:1 and a 4-valve pent-roof cylinder head. A conventional spark-plug ignition system was used for all the experimental tests. The fuel was supplied by two different outwardly opening poppet valve gas injection systems: a PFI system with a maximum injection pressure of 5 bar and a medium-pressure DI injection system with a maximum injection pressure of 30 bar. The DI system ensured that the injection duration was sufficiently short to inject the required fuel quantity when the injection was moved towards the top dead center (TDC). The injection duration was used as a parameter to control the amount of fuel injected.

Table 1
Main engine specifications.

Number of cylinders	1
Number of strokes	4
Displaced volume	454.2 cm^3
Stroke	86.0 mm
Injection systems	PFI-DI
Ignition system	Spark plug
Cylinder diameter	82.0 mm
Compression ratio	10.7
Connecting rod length	144.0 mm
Valves per cylinder	2 intake, 2 exhaust
Engine management system	AVL PREMS GDI
Combustion system	4-valve pent-roof GDI
Intake Valve Opening (IVO)[a]	−380 CAD
Intake Valve Closing (IVC)[a]	−135 CAD
Exhaust Valve Opening (EVO)[a]	−600 CAD
Exhaust Valve Closing (EVC)[a]	−338 CAD

[a] With respect to the firing TDC (0 CAD).

Fig. 1 depicts a sketch of the test cell utilized in this experimental research. The original layout of the test bench was modified to accommodate hydrogen operation. To ensure safety, a flame arrester was installed in the intake manifold upstream of the EGR mixer, and a dedicated hydrogen supplier system was implemented to furnish the injectors.

The experimental facility enables comprehensive control of each relevant parameter during engine operation. High-diluted air conditions were achieved using an external compressor, while an exhaust back-pressure control was achieved through a knife-gate valve located on the exhaust line. Automated valves were employed to manage the hydrogen injection pressure when transitioning between PFI and DI modes.

The test bench is fully equipped with state-of-the-art measurement devices. A piezoelectric sensor was used to measure in-cylinder pressure, and two different piezoresistive sensors were utilized to measure

Table 2
Instrumentation accuracy.

Signal (High frequency)	Sensor	Specification	Accuracy
In-cylinder pressure	Piezoelectric sensor	0 to 250 bar ± 0.3% linearity	±0.8%
Intake pressure	Piezoresistive sensor	0 to 10 ± 0.001 bar	±0.8%
Exhaust pressure	Piezoresistive sensor	0 to 10 ± 0.001 bar	±0.8%
Variable (Low frequency)	**Sensor**	**Specification**	**Accuracy**
Engine speed	Optical angular encoder	1 to 6000 ± 1 rpm	±0.1%
Engine torque	Strain-gauges torque-meter	−200 to 200 ± 1 N m	±0.4%
Intake pressure	Piezoresistive transducer	0 to 10 bar ± 1%	±0.8%
Exhaust pressure	Piezoresistive transducer	0 to 10 bar ± 0.3%	±0.8%
Intake temperature	Thermocouple type K	0 to 1000 ± 0.5 °C	±1.0%
Exhaust temperature	Thermocouple type K	0 to 1000 ± 0.5 °C	±1.0%
Fluid temperature	Pt100 thermoresistance	−200 to 850 ± 0.3 °C	±0.6%
Air mass flow	Air flow meter	0.6–100 m^3/h ± 1%	±1.0%
Hydrogen mass flow	Thermal mass flow meter	200–1600 l/min (based on N_2) ± 0.5%	±0.1%

Table 3
Accuracy levels of HORIBA MEXA 7100 DEGR for measurements of gaseous species.

Pollutant	Analyzer	Range	Accuracy
HC	FID	Min. 0 to 10 ppm C Max. 0 to 50 kppm C	±3%
NO_x	CLD	min. 0 to 10 ppm Max. 0 to 10 kppm C	±3%
CO	NDIR	min. 0 to 3 kppm C Max. 0 to 12 vol%	±3%
CO_2	NDIR	Min. 0 to 5 kppm C Max. 0 to 20 vol%	±3%
O_2	PMA	Min. 0 to 5 vol% Max. 0 to 25 vol%	±3%

intake and exhaust pressures. The Bronkhorst F-113AC-1M0-AAD-55-V flowmeter was employed to register the hydrogen flow rate. All signals were recorded at a sampling frequency of 0.2 CAD. For the analysis of NO_x emissions and other relevant exhaust gases, a HORIBA MEXA-7600EGR equipment was utilized. The accuracy of the main instrumentation is presented in Tables 2 and 3. The measurement equipment employed in this study is state-of-the-art technology in the field of ICE research, and the measurement protocol is sufficiently robust and reliable to trust the obtained results.

The IMEP, cycle-to-cycle variability (CCV) expressed by the IMEP coefficient of variation (COV_{IMEP}), emissions, and indicated efficiency levels were determined using a specialized in-house combustion diagnosis tool [44,45], which was specifically adapted for hydrogen fuel usage. The software incorporated an estimation of combustion efficiency by analyzing the oxygen measurements in the exhaust. This estimation accounted for the excess oxygen corresponding to the air dilution ratio and other contaminants that rely on oxygen for their formation, such as NO_x.

2.2. Experimental method

The aforementioned facility served as the primary tool for the investigation. The experimental campaign involved measuring various conditions at two relevant operating points, characterized by 4 bar and 7 bar of IMEP while running at 1500 rpm (referred to as 1500@4 and 1500@7). A summary of all operating point conditions is presented in Table 4.

The IMEP targets were established by operating the engine with a reference air-to-fuel ratio and the PFI configuration. Once the desired load level was achieved, the fuel quantity was recorded and used in subsequent tests conducted for a given operating point. In this regard, the injected fuel mass was adjusted to maintain the same energy available for combustion at that specific load level. It should be noted that under these conditions, the IMEP level may vary if the thermal efficiency changes due to modifications in other parameters, such as the dilution ratio or combustion phasing. Therefore, the target values of engine load used to designate the operating points should be considered qualitative references that simply indicate whether the engine load is low or medium.

Table 4
Testing conditions and operating points.

Operating point	λ [–]	Injection system	SoI [CAD aTDC]
1500@4	2.2:0.2:3.2 2.6	PFI/DI DI	−340/−130 [−340:10:−40]
1500@7	2.2:0.2:3.2 2.6	PFI/DI DI	−340/−130 [−130:10:−85]

The external air compressor was employed to regulate the amount of air and achieve the desired dilution ratios. The backpressure was maintained at 0.1 bar higher than the intake pressure to mimic realistic conditions at the turbine entry. The energy deposition supplied by the spark plug remained constant throughout all tests. The intake temperature, measured at the surge tank, was set at 308.2 K, while the oil and coolant temperatures were maintained at a constant 363.2 K. The measurement process followed a rigorous protocol, including three repetitions for each considered operating condition. Measurements were only accepted when the variation of key variables was within the uncertainty of the sensor or they did not exhibit a deviation greater than 2% compared to the other repetitions. The controlled variables were: engine speed, engine torque, intake/exhaust pressures, air mass flow, hydrogen mass flow, indicated mean effective pressure (IMEP), COV_{IMEP}, combustion phasing (CA50) and NO_x levels. All high-frequency signals were sampled with a resolution of 0.2 CAD. The results presented in the following sections represent the average value obtained from these three repetitions, with each repetition consisting of 250 engine cycles.

Two studies were proposed: a comparison of the injection systems under identical conditions of fuel-air mixture and load, and an examination of how the injection timing influences the engine emissions and performance. The first study was conducted within a range of λ (2.2 to 3.2) values where emissions and engine performance are analyzed. The second study involved sweeping the injection timing, ranging from the start of the intake stroke when the intake valve is open to as close as possible to the firing TDC during the compression stroke. This range covered both valve-open and valve-closed injection with the DI injector, limited by misfiring.

3. Results and discussion

This section presents the results obtained from the application of the methodology described. The analysis is divided into two subsections, corresponding to the two studies outlined in the previous section.

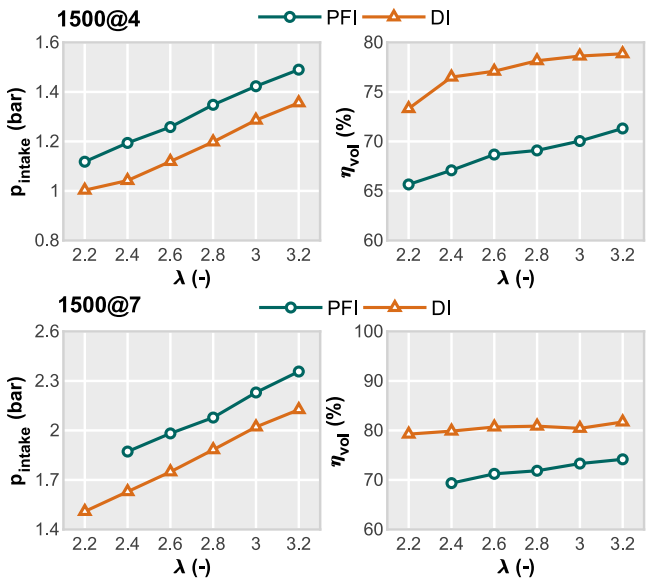

Fig. 2. Impact of the injection system on intake pressure and volumetric efficiency for different air-to-fuel ratios.

3.1. Comparative analysis of PFI and DI hydrogen systems

The objective of this study is to compare the PFI and DI injection systems under homogeneous charge-lean combustion conditions. To achieve this goal, results from both systems are presented at various air dilution ratios. To ensure the utmost air-fuel mixture homogeneity, the injection timing was set to −130 CAD aTDC, immediately following the IVC. This enabled the analysis of the impact on volumetric efficiency by eliminating hydrogen from the intake ports.

The impact of the injection system on intake pressure and the volumetric performance of the engine is illustrated in Fig. 2. In this figure, both PFI and DI systems were used for different combinations of engine load and air-to-fuel ratios. For both operating points analyzed, the spark timing was optimized to minimize specific fuel consumption (ISFC).

The results demonstrate a consistent decrease in intake pressure when utilizing the DI system, with a difference of approximately 0.2 bar compared to the PFI system along the whole range of dilution ratio. This reduction in intake pressure is directly linked to the enhanced volumetric efficiency observed. Such an effect, which stands as one of the primary advantages of DI systems, was also identified by Maio et al. [37].

This advantage allows the DI system to overcome the limitations associated with the PFI system, which stem from the low density of hydrogen. By improving the engine power output, the DI system also enables the attainment of higher dilution ratios under identical boosting conditions, increments of around 16%–17% of dilution are found by injecting hydrogen with the DI system.

To observe the impact of the injector system on engine performance, Fig. 3 depicts the key engine outputs. As evident from the figure, the DI system yields higher performance levels for both operating conditions. At the operating point of 1500@4, consistent improvements of 4% in IMEP (with PFI system results used as a reference) are observed across all air dilution values. The minimum ISFC is achieved at $\lambda = 3.2$ for both systems, with values of 75.2 g/kWh for PFI and 72.9 g/kWh for DI. In this operating condition, higher dilution conditions for DI have the potential to yield further efficiency gains. At $\lambda = 3.2$, an efficiency of 41.2% is achieved, and the trend suggests that the efficiency may continue to increase, while for PFI, no efficiency values above 40% are reached. Similar gross indicated efficiency (GIE) values are attained

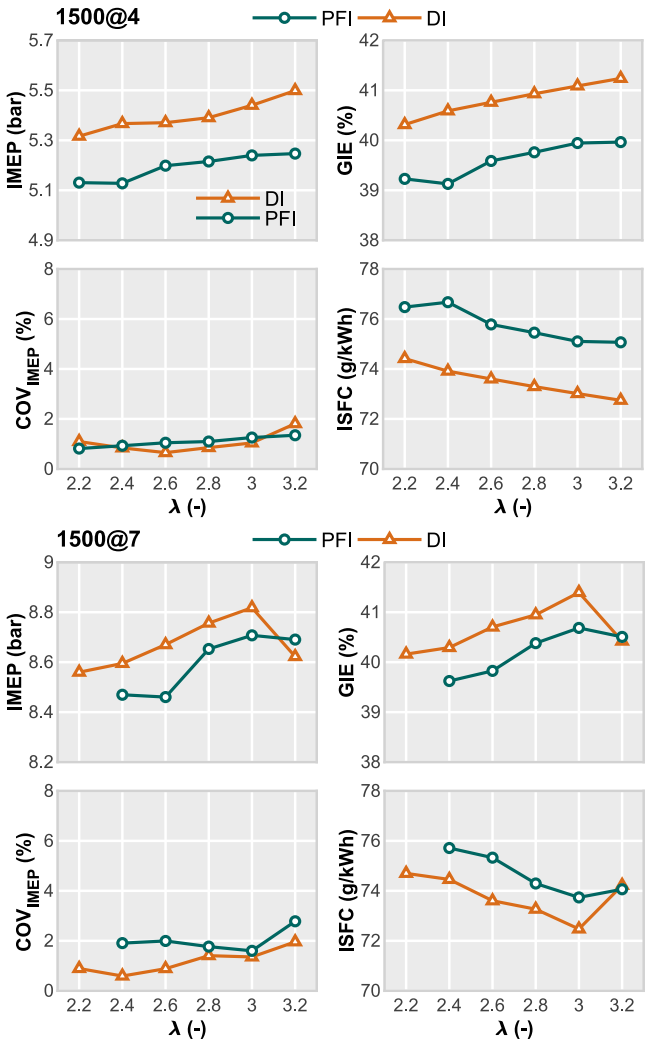

Fig. 3. Impact of the injection system on the performance level for different air-to-fuel ratios.

at $\lambda = 3.0$ and 3.2, indicating a performance peak with respect to air dilution. COV_{IMEP} remains below 2% for all λ cases in both PFI and DI systems, indicating consistent combustion stability.

Moreover, the use of a direct injection system enables operation at lower minimum λ values even under higher engine loads. This feature helps to mitigate the increased tendency for abnormal combustion events and enables an increase in maximum engine torque [20]. For instance, at the operating point of 1500@7, knocking conditions were found with PFI injection when λ is reduced up to 2.2, while the DI system was able to operate without knocking in these particular dilution conditions. The specified operating condition for the PFI system could not be measured as the knock intensity was alarmingly high, even at $\lambda = 2.3$.

At this operating condition, the DI system demonstrated the highest performance, although not equally distributed across the λ range as observed at 1500@4. The maximum IMEP was achieved at $\lambda = 3.0$ for both injection strategies, reaching 8.9 bar for DI and 8.7 bar for PFI. This difference translates to a 1% GIE gain. The maximum performance is achieved at $\lambda = 3.0$, after which the performance declines for the DI system. In contrast, when utilizing the PFI system, the peak IMEP values are attained within the λ range of 2.8 to 3.2. These values stabilize at approximately 8.7 bar of IMEP, signifying a notable 2.4% increase in comparison to λ levels of 2.4 and 2.2. The maximum peak in GIE for 1500@7 is around 0.2%–0.5% higher for both injection systems

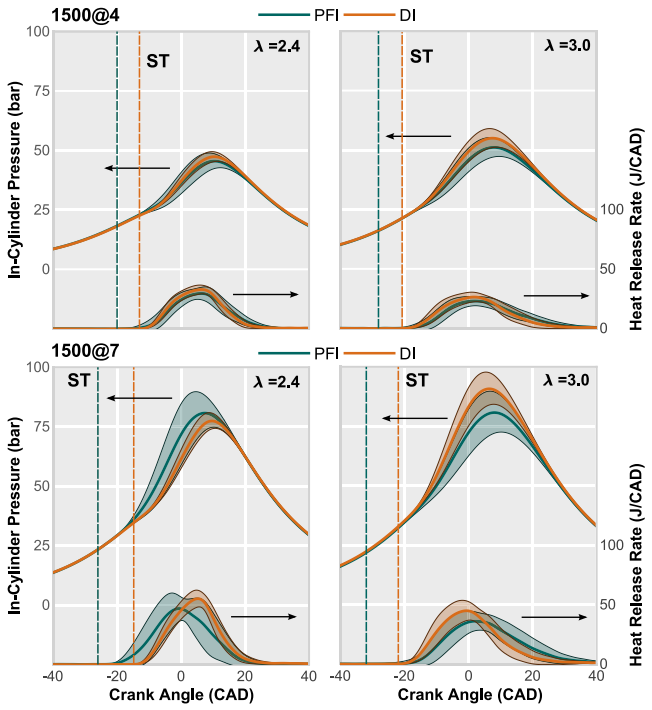

Fig. 4. In-cylinder pressure and HRR profiles for different λ values (2.4 and 3.0) and operating points (1500@4 and 1500@7).

compared to 1500@4, with DI achieving 41.5% and PFI reaching approximately 40.5%. For the PFI system, COV_{IMEP} results are observed to be above the DI system results, reaching a 1% difference at some λ values, although both remain below the instability limit.

The DI system demonstrates performance advantages over the PFI system at 1500@7, although these benefits are lower compared to 1500@4. These variations in performance are discussed from a combustion perspective, considering the in-cylinder pressure and heat release rate (HRR) profiles displayed in Fig. 4. The in-cylinder pressure was averaged per cycle over 250 engine cycles, and the point-to-point standard deviation was included (shadow zones) to illustrate cyclic variation. These data were obtained by using both PFI and DI systems under different air dilution conditions (λ = 2.4 and 3.0) and load conditions. The average cycle is shown, along with the point-to-point standard deviation (SD), which takes into account the CCV. The dashed line indicates the crank angle of the spark discharge.

As can be observed, the in-cylinder pressure profiles from the DI and PFI systems overlap during the compression stroke due to the identical air-fuel mixture conditions enforced in both scenarios. However, the gap between the spark timing and the start of combustion (SOC) is consistently larger in PFI compared to DI. It is worth noting that in DI, the HRR profile increases immediately after the spark timing, whereas in PFI, it takes some time (5 to 10 CAD). Additionally, at low engine load, the HRR profiles resemble each other in terms of peak and duration, while at high load, they exhibit noticeable differences. The combustion duration is significantly shorter in DI, accompanied by a higher HRR peak above 10 J/CAD.

In terms of CCV, both systems demonstrate comparable values at low-load operating points; however, they exhibit substantial differences at higher loads. Specifically, DI exhibits a lower cycle-to-cycle variation, particularly at a lower air-to-fuel ratio (λ = 2.4). Furthermore, an incremental trend is observed in the standard deviation of the HRR profiles, starting with low values and increasing as the crank angle advances. In contrast to the results of the DI system, the PFI system exhibits an approximately constant and higher standard deviation. This fact suggests that the SOC can be better controlled by the DI system. Note that the point-to-point SD is almost zero at the beginning of combustion when using DI, whereas it starts with larger values in PFI. Additionally, it is worth highlighting that the second hump observed in some HRR traces, specifically those with higher CCV, is not a consequence of abnormal combustion events due to end-gas autoignition. This effect is caused by the averaging procedure, which tends to generate the mentioned second hump in the HRR when there is significant cycle-to-cycle dispersion.

To analyze the combustion process of all the conditions considered in this section, relevant combustion parameters are included in Fig. 5. The error bars included in this figure account for the CCV of the presented parameter. As evident from the data, DI consistently exhibits a 2 CAD shorter combustion duration at all λ values, and an approximately 25% higher peak in HRR, indicating that local temperatures may be higher compared to PFI. The peak values of HRR show a tendency to decrease as the air dilution ratio increases. Additionally, the larger gap in GIE observed between PFI and DI at lower loads (1500@4) can be partially attributed to the improved combustion efficiency displayed in the corresponding figure. While there is an approximate difference of 1.5 percentage points between the two injection systems at low loads (1500@4), no substantial differences are observed at higher loads (1500@7).

Regarding the CCV of these parameters, the error bars show consistent results to those presented in Fig. 4. At low load conditions, differences between PFI and DI are almost negligible over the entire dilution range. However, the CCV of both the maximum HRR peak and CA90-10 seems independent of the dilution rate in the DI system, whereas it tends to increase in the PFI system. In contrast, differences are notably higher in high-load conditions. The maximum HRR peak variation remains almost constant around ±6 J/CAD in all dilution conditions in DI, whereas it increases from ±9 to ±12 J/CAD as dilution increases in PFI. Similarly, the CA90-10 variation is around ±5 CAD in DI and from ±10 to ±14 CAD in PFI.

Focusing on pollutant emissions, the NO_x emissions are presented in Fig. 6. It can be observed that at 1500@7, almost double the specific emission levels are attained compared to 1500@4 at the same λ value. As the load increases, so do the temperatures and pressures in the combustion chamber, leading to the activation of thermal NO_x formation.

Although similar trends are observed between both injection systems, especially at low load conditions, the increase in NO_x starts at λ = 2.8 with PFI whereas this inflection point decreases up to λ = 2.6 with DI. It seems that the particular design of the injector leads to a unique mixture stratification that may influence the λ value at which the NO_x levels start to rise, even if the overall air-to-fuel ratio is the same as the PFI case. Therefore, although injecting just after IVC may seem suitable to achieve a homogeneous mixture in the combustion chamber, it does not appear to be sufficient in cases with high dilution (above λ 2.4) where spark timing must be significantly advanced to achieve optimal combustion phasing. This can be inferred from the CA50 obtained in each of the dilution conditions and injection systems represented in Fig. 6. Focusing on the dilution range where NO_x levels are very close to 0 (λ = 2.6 for DI and λ = 2.8 for PFI), it can be seen that the CA50 hardly changes in PFI, while it advances from 6 CAD after TDC to 4 CAD before TDC. This suggests that the mixture distribution in the combustion chamber at the spark timing favors combustion with lower local temperatures, leading to a reduction in NO_x comparable to that of λ = 2.8 in PFI. However, this is something that should be verified through advanced numerical simulations where it is possible to observe the equivalence ratio distribution in the chamber.

In any case, it seems that under homogeneous mixing conditions, the DI system should not provide any advantage in terms of emissions. It is necessary to rely on air dilution to lower combustion temperatures and achieve low levels of NO_x emissions.

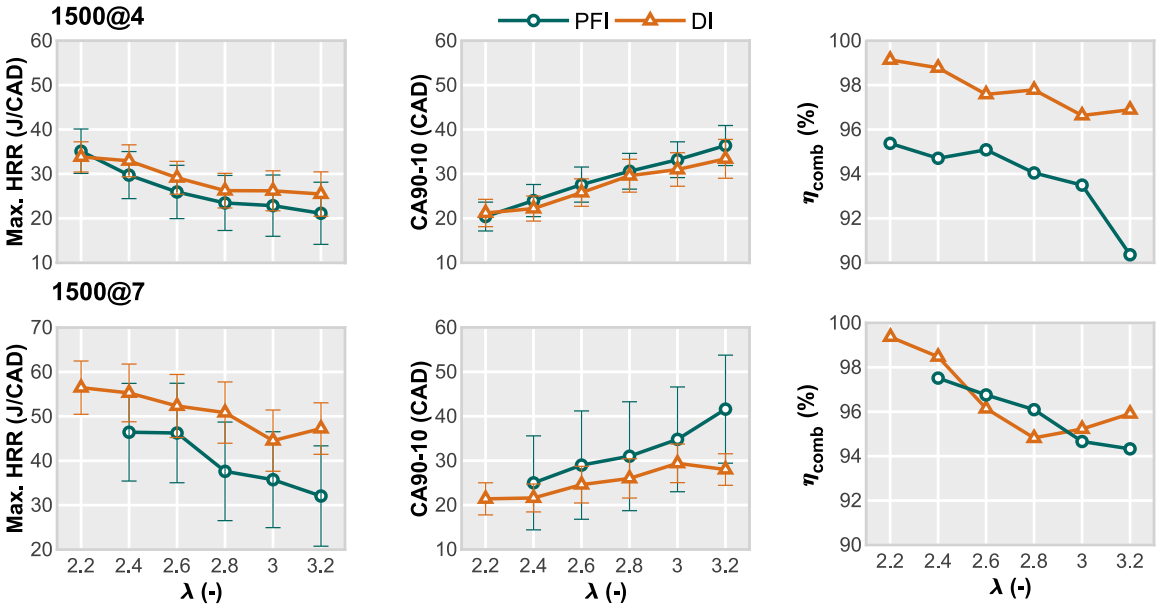

Fig. 5. Impact of the injection system on the combustion performance for different air-to-fuel ratios.

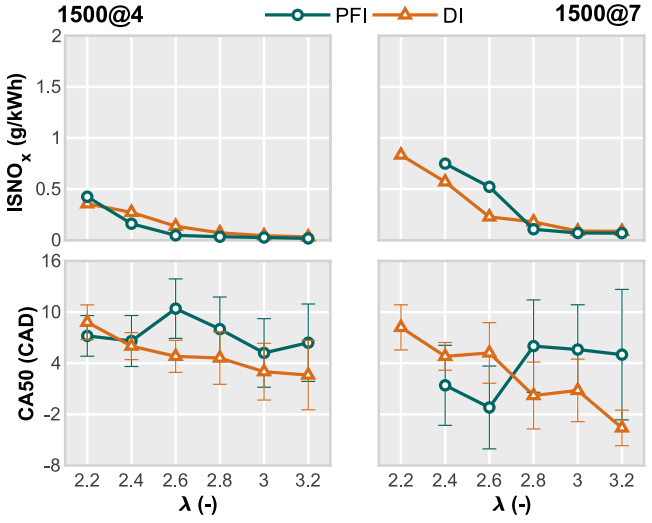

Fig. 6. Impact of the injection system on NO_x emissions and MBT combustion phasing for different air-to-fuel ratios.

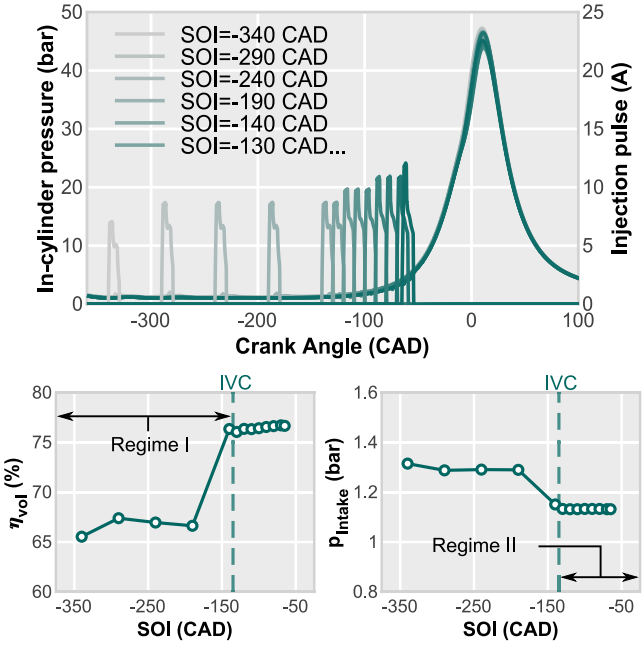

Fig. 7. The impact of injection timing on intake pressure and volumetric efficiency using the DI system under constant λ (2.6) and low-load conditions. In-cylinder pressure profiles have been also included together with the injection pulses for reference.

3.2. Impact of injection timing on H2-DI

The second study focuses on analyzing the impact of injection timing (SoI) using the DI system on engine performance, combustion, and emissions. Initially, the study examines the low-load point (1500@4), where a sweep of start of injection was performed, considering instants during both intake stroke and compression stroke. In this regard, the analysis encompasses a transition from a homogeneous mixture, with the SoI ranging from −340 to −180, to a stratified mixture, with the SoI ranging from −140 to −65.

Fig. 7 illustrates the effect of the SoI on intake pressure and volumetric efficiency. Two different regimes are demarcated by the IVC position. In regime I, the fuel is injected while the intake valve is still open, requiring higher pressure to push the air into the cylinder due to the resistance caused by the low density of hydrogen. Conversely, in regime II, where the start of injection occurs with the intake valves closed, the intake pressure decreases, and the volumetric efficiency increases. In both regimes, the intake pressure remains independent of the SoI, exhibiting a purely binary behavior. It is evident that injecting after the valves closing event has some advantages from the point of view of engine scavenging. However, it may pose disadvantages in terms of mixture formation due to the limited time span between the SoI and the start of combustion.

The most relevant engine performance parameters are plotted in Fig. 8 as the SoI is varied while keeping the air-to-fuel ratio (λ = 2.6) constant. Once again, two distinct trends are observed based on the intake valve closing event. In regime I, the engine performance remains almost constant with SoI retardation. The thermal efficiency is around 40%, and the CCV is below or close to 1%, indicating remarkable operational stability.

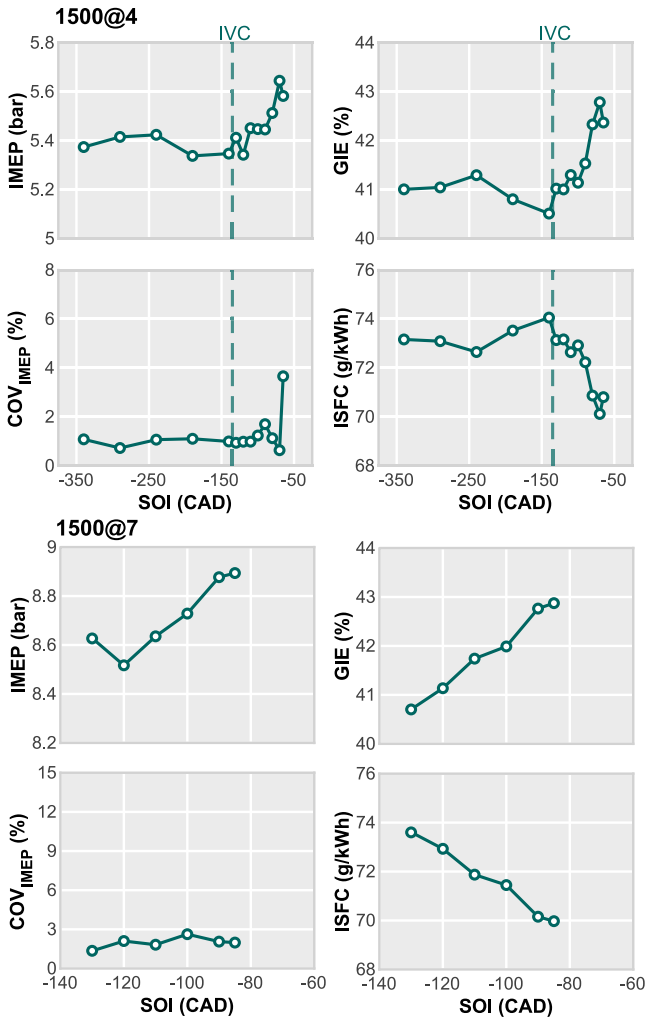

Fig. 8. The impact of injection timing on engine performance parameters using the DI system under constant λ (2.6).

In relation to regime II, delaying the SoI leads to a significant increase in performance. The GIE increases from 40% to nearly 43%, while the CCV remains below 1%–2% (SoI = −70 CAD aTDC). Consequently, the IMEP increases, and the ISFC decreases to 70 g/kWh, indicating a 0.1% improvement in ISFC per degree of delayed SoI. However, a peak of instability is observed when injection starts at −65 CAD aTDC. At this point, the CCV increases up to 4% and the GIE slightly decreases, indicating that the peak performance has been reached. However, what is truly intriguing is what the graph does not reveal. The subsequent SoI (−60 CAD aTDC) could not be measured due to the high CCV, which jeopardized operational stability as a result of excessive misfiring cycles. This implies that crucial factors such as mixing preparation, flow velocity field, and turbulence levels within the combustion chamber are being impacted by late injection, exerting a negative influence on combustion stability.

To conduct a comprehensive analysis of this specific behavior, Fig. 9 depicts the maximum in-cylinder peak pressure for all recorded cycles. The plot illustrates the relationship between the peak pressure and its angular position for the two most delayed SoI cases (−70 and −65 CAD aTDC). This visualization allows us to observe how combustion deteriorates as the SoI is delayed closer to top dead center.

The plot reveals that combustion deterioration occurs with a relatively minor variation of SoI. The measured cycles transition from exhibiting low cycle-to-cycle variation (SoI = −70 CAD aTDC) to compromising engine stability in a span of fewer than 10 CAD of injection

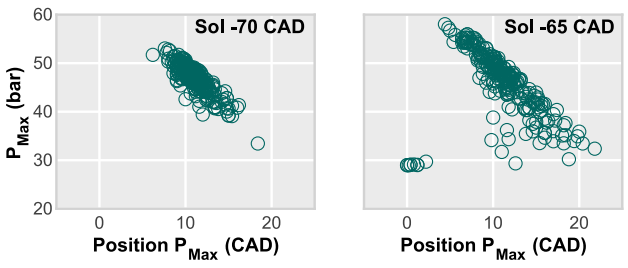

Fig. 9. Cycle-to-cycle variation for extreme SoI conditions (−70 and −65 CAD aTDC). The plot illustrates the maximum peak pressure inside the cylinder against its angular position for the low load case (1500@4) at λ = 2.6.

delay. The repetitiveness of the pressure peaks is evident at SoI = −70 CAD, where a strong correlation between these peaks and their angular position is observed. This indicates consistent combustion velocity for each cycle. However, for the delayed SoI case, this relationship is less clear, suggesting issues with initial flame development in multiple engine cycles. Some of these cycles even exhibit complete misfiring, with maximum pressure peaks approaching values attained during motored conditions at TDC (approximately 30 bar).

The examination of the high load point (1500@7) results in Fig. 8, also revealing similar trends as the low load case (1500@4). In this instance, the sweep of the SoI was performed between −130 and −85 CAD aTDC, considering only the observed regime II when injection occurs during the compression stroke. Once again, a significant gain in thermal efficiency is observed, with GIE increasing from nearly 41% to 43%. The ISFC can be decreased to 70 g/kWh while maintaining the COV$_{IMEP}$ around 2%. The only difference is in the maximum allowable delay for the start of injection before combustion stability is lost. While the low load point allowed an injection timing of −65 CAD aTDC, this higher load point cannot sustain stable operation with further delays beyond −85 CAD aTDC.

To investigate the underlying cause of this specific behavior, Fig. 10 provides an overview of the combustion periods gathered by the spark timing (ST), CA10, CA50, and CA90. This representation, derived from the cycle-averaged heat release rate profiles, facilitates the analysis of how combustion is influenced by the injection event. Examining the data for the 1500@4 point, the results demonstrate that delaying the injection up to −70 CAD aTDC leads to an acceleration of combustion during the initial stages (ST-CA10 and CA10-CA50), indicating improved mixing and turbulence conditions in the vicinity of the spark plug. However, with further injection delays, combustion deteriorates across all stages. It is noteworthy that all the depicted stages lengthen with the SoI at −65 CAD aTDC. This behavior, however, is not precisely replicated at higher loads. Transitioning from a stable SoI (−130 CAD aTDC) to the most delayed SoI (−85 CAD aTDC) reveals that the burning rate remains largely unchanged during the early stages of combustion, while the third stage (CA50-CA90) elongates, indicating that combustion instability has shifted towards the latter part of the combustion process.

This phenomenon can be attributed to multiple factors, including inadequate turbulence in the combustion chamber, which hampers the effective mixing of fuel and air as well as the propagation of the turbulent flame. Additionally, inappropriate matching between the injector and chamber design could also contribute to this issue. Regrettably, in order to gain a comprehensive understanding of the influence of injection timing on combustion stability and efficiency, as well as to develop strategies for optimizing injection timing under diverse operating conditions, further research is required. This research should involve advanced optical techniques and/or numerical models to delve deeper into the subject matter and are out of the scope of this investigation.

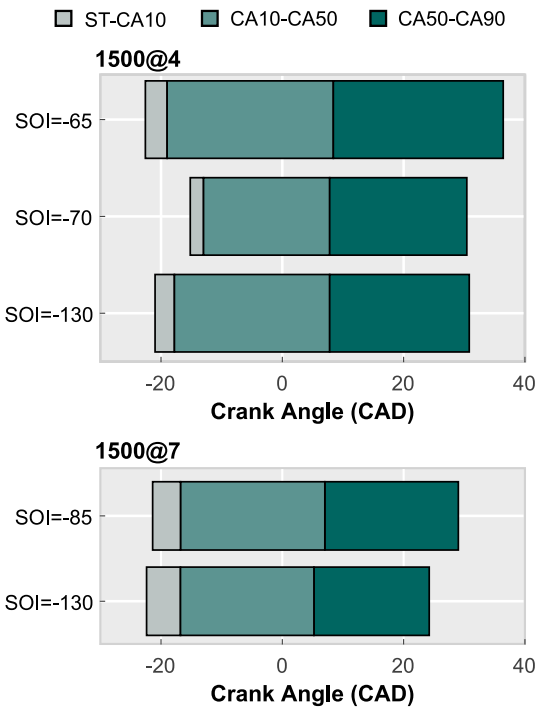

Fig. 10. Combustion periods for different SoI and load conditions operating at λ = 2.6.

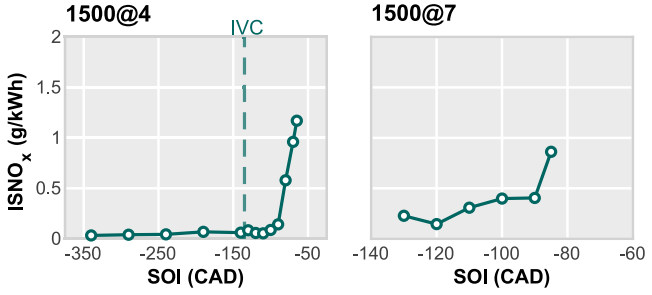

Fig. 11. NO_x emission levels for different SoI and load conditions operating at λ = 2.6.

To assess the influence of these combustion variations on pollutant levels, the results of NO_x emissions are presented in Fig. 11 for both load levels operating at $\lambda = 2.6$. It can be observed that NO_x emissions remain consistently low throughout most of the SoI sweep, primarily due to the inhibitory effect of high dilution rates on NO_x formation through the thermal mechanism. However, as the injection is further delayed beyond −110 CAD a TDC during low load conditions, a noticeable increase in NO_x emissions becomes evident. This trend suggests the onset of stratified charge, where a locally richer mixture forms, leading to higher flame temperatures and subsequently increased NO_x production. At the 1500@7 load point, NO_x levels are slightly elevated but still below 0.5 g/kWh before experiencing a sharp increase due to mixture inhomogeneity. In this particular case, the turning point occurs at −90 CAD aTDC.

This trend contradicts the performance gains observed in Fig. 8. Therefore, understanding the source of this efficiency improvement can aid in resolving this issue. Examining the pressure-volume diagrams presented in Fig. 12 for the low load point provides insight into how the compression work is affected as the injection is shifted towards TDC. It can be observed that as the injection is delayed, the compression work is reduced. Computing this parameter at −20 CAD aTDC (ensuring that combustion is not initiated in all considered points), there is a 7.6%

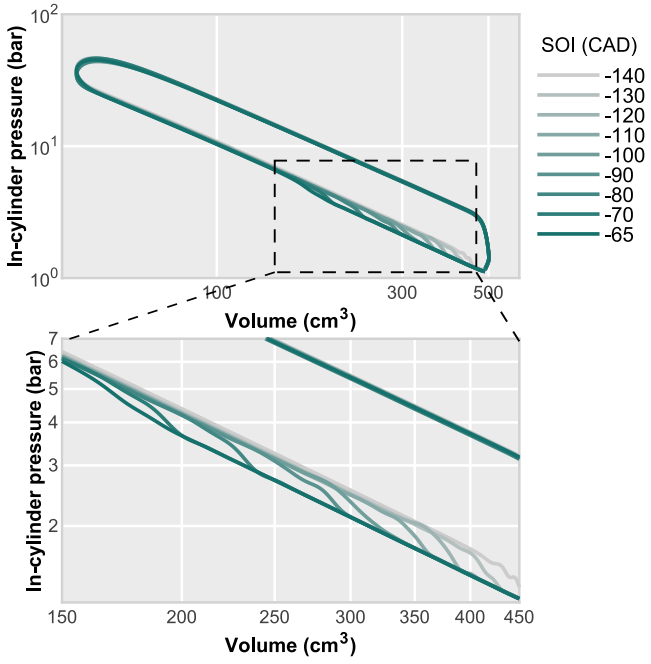

Fig. 12. P-V diagrams for the SoI sweep at λ = 2.6 cases. The pumping losses were not included to evaluate only the work produced in the firing cycle.

reduction at low load and a 3.9% reduction at high load before compromising combustion stability. This translates to the observed 3.1–3.2% improvement in ISFC (Fig. 8) for both load conditions considered. The area of this diagram, corresponding to the indicated work, increases with injection delay. This effect is amplified by the low density of hydrogen, which makes it more prominent compared to other gaseous fuels such as natural gas.

These findings carry significant implications for the design and optimization of DI hydrogen combustion engines, emphasizing the crucial role of precise injection timing control in achieving both high performance and low emissions. Moreover, this study underscores the necessity for further research to examine the effects of delayed injection on emissions and combustion stability.

3.3. Comparison with other fuels and injection technologies

This concluding section summarizes the performance and emissions levels achieved when utilizing hydrogen as fuel in a spark-ignition engine, emphasizing significant findings relevant to the advancement of hydrogen-powered engines. Additionally, a comparison is drawn between hydrogen and conventional fuels, such as gasoline and compressed natural gas which are commercially available at present. This comparison is feasible as equivalent operating conditions to those employed in this study were measured for gasoline and CNG under PFI conditions. The engine measurements utilizing both gasoline and CNG were carried out on the same engine and under identical operating conditions. These datasets have already been published in previous works [11,43] and serve as baseline tests for comparison with conventional fuels. To achieve this, the authors maintained consistent operating conditions, including engine speed and load, while adjusting the fuel injected mass to ensure the total energy available for combustion remained constant.

The comparison of the results shown in Fig. 13 highlights that hydrogen engines have the potential to outperform gasoline and CNG engines. This can be attributed to their higher efficiency and lower GHG and pollutant emissions. NO_x can be effectively controlled by implementing high dilution levels, which in turn enable the attainment

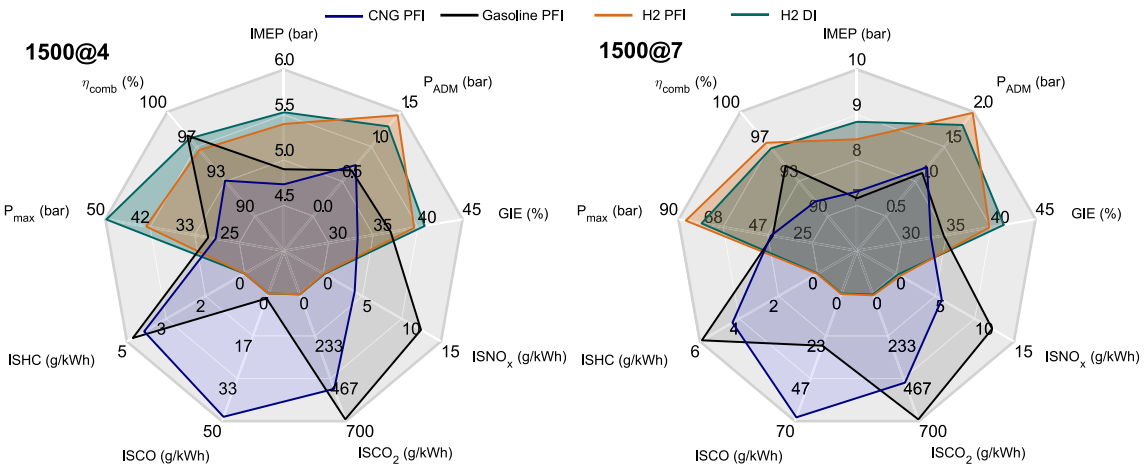

Fig. 13. Comparison between the engine most significant parameters when operating with hydrogen and conventional fuels like gasoline and CNG.

of high thermal efficiency while preserving combustion stability. Moreover, this approach helps maintain very low levels of hydrocarbon (HC) and carbon monoxide (CO) emissions (although not reaching zero due to potential interactions with the oil).

As depicted in Fig. 13, there is a paradigm shift where emissions are effectively controlled, resulting in improved efficiency and reduced fuel consumption. However, this shift presents various technological challenges. These include the need for turbocharging systems that can handle high intake pressures in PFI systems, injectors capable of operating with low-density fluids and moderate backpressure chamber pressures, as well as addressing issues related to distribution and storage, among others.

In contrast, gasoline and CNG enjoy wide availability and can offer short-term cost-effectiveness. However, the environmental advantages of hydrogen and CNG should not be overlooked, as their utilization can contribute to the reduction of greenhouse gas emissions in the transportation sector. Therefore, a practical solution for achieving a balance between performance and sustainability during the transition towards a more environmentally friendly future could involve a combination of fuels, such as hydrogen blends or hybrid systems.

4. Conclusions

The study explores the potential of using a modern spark ignition engine with an outwardly opening poppet valve hydrogen injector. To achieve this, two different injection technologies–PFI and DI–are implemented in a single-cylinder SI engine. The comparison of emission levels, performance, and combustion characteristics has been conducted under various dilution, load, and injection timing conditions. Overall, this study provides valuable insights into the use of such injectors for internal combustion engines in light-duty applications and highlights key areas for future research.

The results demonstrate that the direct injection system outperforms the port fuel injection system along the entire range of air dilutions considered in this study. Gains of approximately 0.6 to 1.1% in gross indicated efficiency are observed at the two load conditions considered. Additionally, the direct injection system exhibits the advantage of requiring a lower intake pressure when the injection timing is set after the intake valves closing event, thereby alleviating the stress on the boosting system.

In terms of NO_x emissions, both injection systems achieve similar levels and trends, although some differences can be found at high load. The injector-specific design seems to create a distinct mixture stratification, potentially impacting the λ at which NO_x levels rise, despite an identical overall air-to-fuel ratio compared to the PFI case.

A precise injection timing control is crucial to achieving both high performance and low emissions in DI hydrogen combustion engines. Delaying the start of injection results in a 7.6% reduction in compression work at low load and a 3.9% reduction at high load before compromising combustion stability. This results in a 3.1–3.2% improvement in ISFC in both load conditions considered. However, this action also results in a reduced mixing time, which leads to charge stratification. This effect contributes to increased NO_x emissions, as hydrogen is burned under richer conditions compared to the overall dilution condition.

The conclusions of this research should be considered as an initial starting point for future investigations since some of the conclusions presented here are completely based on experimental observations, which can make it challenging to provide a comprehensive explanation of the observed trends. Results evinced that understanding the local thermodynamic conditions within the combustion chamber is crucial for achieving stable flame development. Similarly, it is essential to manage the local equivalence ratios effectively in order to control the production of NO_x.

Therefore, further research should combine experimentation with simulations to understand and overcome these limitations. In this context, a deeper understanding of local phenomena can lead to substantial reductions in cooling losses and improvements in thermal efficiency. This involves promoting a lean local mixture fraction near the wall region while simultaneously maintaining a uniformly distributed and sufficiently high air-to-fuel ratio to prevent NO_x production.

CRediT authorship contribution statement

S. Molina: Supervision, Resources, Funding acquisition. **R. Novella:** Supervision, Resources, Methodology, Funding acquisition, Conceptualization. **J. Gomez-Soriano:** Writing – review & editing, Supervision, Methodology, Investigation, Formal analysis, Data curation, Conceptualization. **M. Olcina-Girona:** Writing – original draft, Visualization, Validation, Methodology, Investigation, Data curation.

Declaration of competing interest

The authors declare that they have no known competing financial interests or personal relationships that could have appeared to influence the work reported in this paper.

Data availability

Data will be made available on request.

Acknowledgments

The authors would like to express their gratitude to BORGWARNER for generously providing the medium pressure hydrogen injector.

The authors wish to thank Mr. Gabriel Alcantarilla for his inestimable assistance during the experimental campaign.

Funding

This research has been partially funded by Agencia Estatal de Investigación of the Spanish Government through project TED2021-130596B-C21 (BIOH2FUEL).

M. Olcina-Girona is partly supported by the grant CIACIF/2021/437 of the "Subvenciones para la contratación de personal investigador predoctoral (ACIF)" of the Conselleria d'Innovació, Universitats, Ciència i Societat Digital de la Generalitat Valenciana.

Funding for open access charge: CRUE-Universitat Politècnica de València

References

[1] Fuel Cells and Hydrogen Joint Undertaking (FCH). Hydrogen roadmap europe: a sustainable pathway for the european energy transition. vol. 2019, Luxembourg: Publications Office of the European Union; 2019, p. 70.

[2] Zhang B, Chen Y, Jiang Y, Lu W, Liu W. Effect of compression ratio and miller cycle on performance of methanol engine under medium and low loads. Fuel 2023;351:128985.

[3] Novella R, Pastor J, Gomez-Soriano J, Sánchez-Bayona J. Numerical study on the use of ammonia/hydrogen fuel blends for automotive spark-ignition engines. Fuel 2023;351:128945.

[4] Novella R, Gomez-Soriano J, Martínez-Hernández PJ, Libert C, Rampanarivo F. Improving the performance of the passive pre-chamber ignition concept for spark-ignition engines fueled with natural gas. Fuel 2021;290:119971.

[5] Garcia-Oliver JM, Niki Y, Rajasegar R, Novella R, Gomez-Soriano J, Martinez-Hernandiz PJ, Li Z, Musculus MP. An experimental and one-dimensional modeling analysis of turbulent gas ejection in pre-chamber engines. Fuel 2021;299:120861.

[6] Al-Orabi AM, Osman MG, Sedhom BE. Analysis of the economic and technological viability of producing green hydrogen with renewable energy sources in a variety of climates to reduce CO2 emissions: A case study in Egypt. Appl Energy 2023;338(March):120958. http://dx.doi.org/10.1016/j.apenergy.2023.120958.

[7] Zhang L, Jia C, Bai F, Wang W, An S, Zhao K, Li Z, Li J, Sun H. A comprehensive review of the promising clean energy carrier: Hydrogen production, transportation, storage, and utilization (HPTSU) technologies. Fuel 2024;355(2023):129455. http://dx.doi.org/10.1016/j.fuel.2023.129455.

[8] Danieli P, Lazzaretto A, Al-Zaili J, Sayma A, Masi M, Carraro G. The potential of the natural gas grid to accommodate hydrogen as an energy vector in transition towards a fully renewable energy system. Appl Energy 2022;313(March):118843. http://dx.doi.org/10.1016/j.apenergy.2022.118843.

[9] Benajes J, Novella R, Gomez-Soriano J, Barbery I, Libert C. Advantages of hydrogen addition in a passive pre-chamber ignited si engine for passenger car applications. Int J Energy Res 2021;45(9):13219–37.

[10] Qian L, Wan J, Qian Y, Sun Y, Zhuang Y. Experimental investigation of water injection and spark timing effects on combustion and emissions of a hybrid hydrogen-gasoline engine. Fuel 2022;322(April):124051. http://dx.doi.org/10.1016/j.fuel.2022.124051.

[11] Molina S, Ruiz S, Gomez-Soriano J, Olcina-Girona M. Impact of hydrogen substitution for stable lean operation on spark ignition engines fueled by compressed natural gas. Results Eng 2023;17:100799. http://dx.doi.org/10.1016/j.rineng.2022.100799, URL https://www.sciencedirect.com/science/article/pii/S2590123022004698.

[12] Liu W, Qi Y, Zhang R, Zhang Q, Wang Z. Hydrogen production from ammonia-rich combustion for fuel reforming under high temperature and high pressure conditions. Fuel 2022;327:124830.

[13] Zhang H, Li G, Long Y, Zhang Z, Wei W, Zhou M, Belal BY. Numerical study on combustion and emission characteristics of a spark-ignition ammonia engine added with hydrogen-rich gas from exhaust-fuel reforming. Fuel 2023;332:125939.

[14] Verhelst S, Wallner T. Hydrogen-fueled internal combustion engines. Prog Energy Combust Sci 2009;35(6):490–527. http://dx.doi.org/10.1016/j.pecs.2009.08.001.

[15] zhi Bao L, gang Sun B, he Luo Q. Experimental investigation of the achieving methods and the working characteristics of a near-zero NOx emission turbocharged direct-injection hydrogen engine. Fuel 2022;319(February):123746. http://dx.doi.org/10.1016/j.fuel.2022.123746.

[16] zhi Bao L, gang Sun B, he Luo Q. Optimal control strategy of the turbocharged direct-injection hydrogen engine to achieve near-zero emissions with large power and high brake thermal efficiency. Fuel 2022;325(April):124913. http://dx.doi.org/10.1016/j.fuel.2022.124913.

[17] zhi Bao L, gang Sun B, he Luo Q, cheng Li J, chao Qian D, yang Ma H, jun Guo Y. Development of a turbocharged direct-injection hydrogen engine to achieve clean, efficient, and high-power performance. Fuel 2022;324(PB):124713. http://dx.doi.org/10.1016/j.fuel.2022.124713.

[18] Barış O, Güler İ, Yaşgül A. The effect of different charging concepts on hydrogen fuelled internal combustion engines. Fuel 2023;343:127983.

[19] Kim Y, Lee JT, Choi GH. An investigation on the causes of cycle variation in direct injection hydrogen fueled engines. Int J Hydrogen Energy 2005;30(1):69–76.

[20] White C, Steeper R, Lutz A. The hydrogen-fueled internal combustion engine: a technical review. Int J Hydrogen Energy 2006;31(10):1292–305.

[21] Byun CH, Lee JT, Kwon OC. An experimental study on the self-ignition and knocking characteristics for hydrogen-fueled homogeneous compression charge ignition engines. Fuel 2023;351(March):128970. http://dx.doi.org/10.1016/j.fuel.2023.128970.

[22] Verhelst S. Recent progress in the use of hydrogen as a fuel for internal combustion engines. Int J Hydrog Energy 2014;39(2):1071–85.

[23] Gao J, Wang X, Song P, Tian G, Ma C. Review of the backfire occurrences and control strategies for port hydrogen injection internal combustion engines. Fuel 2022;307:121553.

[24] Szwaja S, Naber JD. Dual nature of hydrogen combustion knock. Int J Hydrogen Energy 2013;38(28):12489–96. http://dx.doi.org/10.1016/j.ijhydene.2013.07.036.

[25] Novella R, García A, Gomez-Soriano J, Fogué-Robles Á. Exploring dilution potential for full load operation of medium duty hydrogen engine for the transport sector. Appl Energy 2023;349:121635.

[26] Shi C, Chai S, Wang H, Ji C, Ge Y, Di L. An insight into direct water injection applied on the hydrogen-enriched rotary engine. Fuel 2023;339(2022):127352. http://dx.doi.org/10.1016/j.fuel.2022.127352.

[27] Verhelst S, Maesschalck P, Rombaut N, Sierens R. Increasing the power output of hydrogen internal combustion engines by means of supercharging and exhaust gas recirculation. Int J Hydrogen Energy 2009;34(10):4406–12.

[28] Thawko A, Persy SA, Eyal A, Tartakovsky L. Effects of fuel injection method on energy efficiency and combustion characteristics of SI engine fed with a hydrogen-rich reformate. In: SAE technical papers (2020). 2020, p. 1–12. http://dx.doi.org/10.4271/2020-01-2082.

[29] Gao J, Wang X, Tian G, Song P, Ma C, Huang L. Effect of hydrogen direct injection strategies and ignition timing on hydrogen diffusion, energy distributions and NOx emissions from an opposed rotary piston engine. Fuel 2021;306(May). http://dx.doi.org/10.1016/j.fuel.2021.121656.

[30] Ji C, Hong C, Wang S, Xin G, Meng H, Yang J, Qiang Y. Evaluation of the variable valve timing strategy in a direct-injection hydrogen engine with the miller cycle under lean conditions. Fuel 2023;343(2022):127932. http://dx.doi.org/10.1016/j.fuel.2023.127932.

[31] yu Lai F, gang Sun B, Wang X, sheng Zhang D, he Luo Q, zhi Bao L. Research on the inducing factors and characteristics of knock combustion in a DI hydrogen internal combustion engine in the process of improving performance and thermal efficiency. Int J Hydrogen Energy 2023;48(20):7488–98. http://dx.doi.org/10.1016/j.ijhydene.2022.11.091.

[32] Kaiser S, White CM. PIV and PLIF to evaluate mixture formation in a direct-injection hydrogen-fuelled engine. SAE Int J Engines 2009;1(1):657–68. http://dx.doi.org/10.4271/2008-01-1034.

[33] Salazar VM, Kaiser SA. An optical study of mixture preparation in a hydrogen-fueled engine with direct injection using different nozzle designs. SAE Int J Engines 2010;2(2):119–31. http://dx.doi.org/10.4271/2009-01-2682.

[34] Eichlseder H, Wallner T, Freymann R, Ringler J. The potential of hydrogen internal combustion engines in a future mobility scenario. In: SAE technical paper. Tech. rep., 2003.

[35] Kim Y, Lee JT, Caton JA. The development of a dual-injection hydrogen-fueled engine with high power and high efficiency. J Eng Gas Turb Power 2006;128(1):203–12.

[36] Kim Y, Park C, Oh J, Oh S, Choi Y, Lee J. Effect of excessive air ratio on hydrogen-fueled spark ignition engine with high compression ratio using direct injection system toward higher brake power and thermal efficiency. 2023, Available at SSRN 4012806.

[37] Maio G, Boberic A, Giarracca L, Aubagnac-Karkar D, Colin O, Duffour F, Deppenkemper K, Virnich L, Pischinger S. Experimental and numerical investigation of a direct injection spark ignition hydrogen engine for heavy-duty applications. Int J Hydrogen Energy 2022;47(67):29069–84.

[38] Shudo T, Cheng W, Kuninaga T, Hasegawa T. Reduction of cooling loss in hydrogen combustion by direct injection stratified charge. SAE Trans 2003;2118–23.

[39] Deshmukh AY, Giefer C, Goeb D, Khosravi M, van Bebber D, Pitsch H. A quasi-one-dimensional model for an outwardly opening poppet-type direct gas injector for internal combustion engines. Int J Engine Res 2020;21(8):1493–519.

[40] Deshmukh A, Vishwanathan G, Bode M, Pitsch H, Khosravi M, van Bebber D. Characterization of hollow cone gas jets in the context of direct gas injection in internal combustion engines. SAE Int J Fuels Lubric 2018;11(4):353–78.
[41] Lazzaro M, Catapano F, Sementa P. Experimental characterization of methane direct injection from an outward-opening poppet-valve injector. In: SAE technical paper. 2019.
[42] Molina S, Novella R, Gomez-soriano J, Olcina-girona M. Experimental evaluation of methane-hydrogen mixtures for enabling stable lean combustion in spark-ignition engines for automotive applications. In: SAE technical papers. 2022, p. 1–12. http://dx.doi.org/10.4271/2022-01-0471.Received.
[43] Molina S, Ruiz S, Gomez-Soriano J, Olcina-Girona M. Impact of hydrogen substitution for stable lean operation on spark ignition engines fueled by compressed natural gas. Results Eng 2023;17:100799.
[44] Benajes J, Olmeda P, Martín J, Carreño R. A new methodology for uncertainties characterization in combustion diagnosis and thermodynamic modelling. Appl Therm Eng 2014;71(1):389–99. http://dx.doi.org/10.1016/J.APPLTHERMALENG.2014.07.010.
[45] Payri F, Olmeda P, Martin J, Carreño R. A new tool to perform global energy balances in DI diesel engines. SAE Int J Engines 2014;7(1):43–59. http://dx.doi.org/10.4271/2014-01-0665.